Chemical Science

ROYAL SOCIETY OF CHEMISTRY

EDGE ARTICLE

View Article Online
View Journal | View Issue

Open Access Article. Published on 12 August 2022. Downloaded on 1/22/2026 11:04:29 AM.
This article is licensed under a Creative Commons Attribution-NonCommercial 3.0 Unported Licence.

Check for updates

Cite this: *Chem. Sci.*, 2022, **13**, 11341

All publication charges for this article have been paid for by the Royal Society of Chemistry

Unprecedented pairs of uranium (IV/V) hydroxido and (IV/V/VI) oxido complexes supported by a seven-coordinate cyclen-anchored tris-aryloxide ligand†

Sascha T. Löffler, ‡ Julian Hümmer, ‡ Andreas Scheurer, Frank W. Heinemann and Karsten Meyer *

Received 16th May 2022
Accepted 30th July 2022

DOI: 10.1039/d2sc02736d

rsc.li/chemical-science

We present the synthesis and reactivity of a newly developed, cyclen-based tris-aryloxide ligand precursor, namely cyclen(Me)($^{t\text{-Bu},t\text{-Bu}}$ArOH)$_3$, and its coordination chemistry to uranium. The corresponding uranium(III) complex [U^{III}((OAr$^{t\text{-Bu},t\text{-Bu}}$)$_3$(Me)cyclen)] (**1**) was characterized by ^{1}H NMR analysis, CHN elemental analysis and UV/vis/NIR electronic absorption spectroscopy. Since no single-crystals suitable for X-ray diffraction analysis could be obtained from this precursor, **1** was oxidized with methylene chloride or silver fluoride to yield [(cyclen(Me)($^{t\text{-Bu},t\text{-Bu}}$ArO)$_3$)U^{IV}(X)] (X = Cl (**2**), F (**3**)), which were unambiguously characterized and successfully crystallized to gain insight into the molecular structure by single-crystal X-ray diffraction analysis (SC-XRD). Further, the activation of H_2O and N_2O by **1** is presented, resulting in the U(IV) complex [(cyclen(Me)($^{t\text{-Bu},t\text{-Bu}}$ArO)$_3$)U^{IV}(OH)] (**4**) and the U(V) complex [(cyclen(Me)($^{t\text{-Bu},t\text{-Bu}}$ArO)$_3$)U^{V}(O)] (**6**). Complexes **2**, **3**, **4**, and **6** were characterized by ^{1}H NMR analysis, CHN elemental analysis, UV/vis/NIR electronic absorption spectroscopy, IR vibrational spectroscopy, and SQUID magnetization measurements as well as cyclic voltammetry. Furthermore, chemical oxidation of **3**, **4**, and **6** with AgF or $AgSbF_6$ was achieved leading to complexes [(cyclen(Me)($^{t\text{-Bu},t\text{-Bu}}$ArO)$_3$)U^{V}(F)$_2$] (**5**), [(cyclen(Me)($^{t\text{-Bu},t\text{-Bu}}$ArO)$_3$)U^{V}(OH)][SbF$_6$] (**7**), and [(cyclen(Me)($^{t\text{-Bu},t\text{-Bu}}$ArO)$_3$)U^{VI}(O)][SbF$_6$] (**8**). Finally, reduction of **7** with KC_8 yielded a U(IV) complex, spectroscopically and magnetochemically identified as K[(cyclen(Me)($^{t\text{-Bu},t\text{-Bu}}$ArO)$_3$)U^{IV}(O)].

Introduction

In low oxidation states, uranium complexes are immensely sensitive to even trace amounts of oxygen and/or water and, in uncontrolled reactions, tend to be fully oxidized to U(VI) compounds in the form of the thermodynamically stable uranyl dication $[U^{VI}O_2]^{2+}$.[1–7] Whereas a few reports of the formation and isolation of U(IV) hydroxido compounds exist,[8–15] the controlled reaction with water – in one-electron oxidation processes with the concomitant release of dihydrogen – is only sparsely reported in the literature.[16–19] The first uranium hydroxido complex was reported by Berthet and Ephritikhine in 1993. In a hydrolysis reaction of the uranium(IV) hydrido complex [(C$_5$H$_4$R)$_3$U^{IV}H] (R = *t*-butyl or SiMe$_3$), with 1 equivalent of H_2O in toluene, the hydroxide species [(C$_5$H$_4$R)$_3$U^{IV}OH] (R = *t*-butyl and SiMe$_3$) were obtained.[8] In 1996, Lukens *et al.* reported the formation and characterization of the dinuclear, bis-hydroxido-bridged complexes [{(Cp')$_2$U^{IV}}$_2$(μ-OH)$_2$] (Cp' = 1,3-(Me$_3$Si)$_2$C$_5$H$_3$) and [{(Cp'')$_2$U^{IV}}$_2$(μ-OH)$_2$] (Cp'' = 1,3-(Me$_3$C)$_2$C$_5$H$_3$) from the reaction of [U^{III}(Cp')$_3$] and [{(Cp')$_3$-U^{IV}}$_2$(μ-H)$_2$] with H_2O, respectively.[9] The first example of a crystallographically characterized terminal uranium(IV) hydroxide was given in 2002 by Scott and co-workers. The oxidation of [(NN′$_3$)U^{III}(CH$_2$PMe$_3$)] (NN′$_3$ = N(CH$_2$CH$_2$NSiMe$_2$^{t}Bu)$_3$) resulted in a non-reproducible structural characterization of [(NN′$_3$)U^{IV}(OH)(CH$_2$PMe$_3$)].[10] Besides, only a few further examples of hydroxido compounds are structurally determined, but these examples were obtained from accidental and uncontrolled reactions, which can be traced back to minor impurities of water (moisture) and were not reproducible in most cases.[11,14,15] Ariyaratne *et al.* reported the reaction of [(Cp*)$_2$U^{IV}(Cl)$_2$(HNSPh$_2$)] with 1 equivalent of HNSPh$_2$ × H_2O to give [(Cp*)$_2$-U^{IV}(OH)(Cl)(HNSPh$_2$)]. The terminal hydroxido complex is an intermediate in the formation of the tetra uranium oxido cluster [Cp*(Cl)(HNSPh$_2$)U(μ$_3$-O)(μ$_2$-O)$_2$U(Cl)(HNSPh$_2$)$_2$]$_2$, which forms upon hydrolysis of [(Cp*)$_2$U(Cl)$_2$] with excess HNSPh$_2$ × H_2O.[12]

Hence, up until now, reports of controlled one- or two-electron oxidations of uranium compounds to form defined terminal hydroxido and oxido complexes, even with excess amount of H_2O, still remain scarce, and are of current interest

Friedrich-Alexander-Universität Erlangen-Nürnberg (FAU), Department of Chemistry and Pharmacy, Inorganic Chemistry, Egerlandstraße 1, 91058 Erlangen, Germany. E-mail: karsten.meyer@fau.de

† Electronic supplementary information (ESI) available: [DETAILS]. CCDC 2080557, 2150855–2150860. For ESI and crystallographic data in CIF or other electronic format see https://doi.org/10.1039/d2sc02736d

‡ Both authors contributed equally.

Open Access Article. Published on 12 August 2022. Downloaded on 1/22/2026 11:04:29 AM.
This article is licensed under a Creative Commons Attribution-NonCommercial 3.0 Unported Licence.

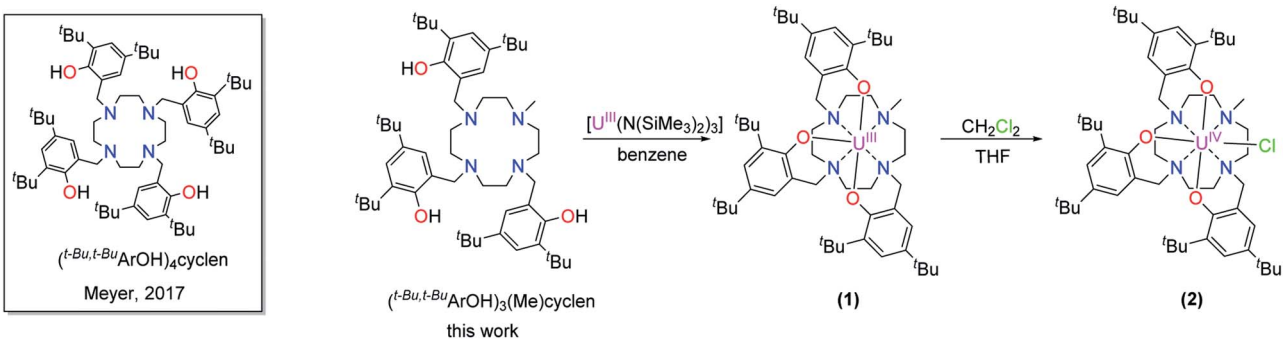

Scheme 1 Synthesis of [U^{III}((OAr$^{t\text{-Bu},t\text{-Bu}}$)$_3$(Me)cyclen)] (**1**) and [(cyclen(Me)($^{t\text{-Bu},t\text{-Bu}}$ArO)$_3$)U^{IV}(Cl)] (**2**).

to our group in the context of the electrocatalytic generation of dihydrogen from water. In 2016, we reported the electrocatalytic production of H_2 mediated by [(mes(^{Ad,Me}ArO)$_3$)U^{IV}(OH)],[16,20] and a series of uranium hydrochalcogenido (EH) and chalcogenido (E) (with E = O, S, Se, Te) uranium(IV) compounds.[18] In the latter report, solutions of [U^{III}((OAr^{Ad,Me})$_3$tacn)] were allowed to react with stoichiometric amounts of the hydrochalcogenides H_2O, H_2S, H_2Se, and H_2Te in THF to obtain the corresponding complexes [(tacn(^{Ad,Me}ArO)$_3$)U^{IV}(EH)]. While the reaction for the higher homologous H_2S, H_2Se and H_2Te is relatively fast, the reaction with H_2O is notably slow, takes at least three days, and the reaction outcome was observed to be the same even when an excess of H_2O was used.[17,18]

In contrast to the stable uranyl dication [U^{VI}O$_2$]$^{2+}$, complexes of uranium with reactive terminal oxido ligands – of which [(mes(^{Ad,Me}ArO)$_3$)U^{V}(O)] has been identified as an intermediate in the above-mentioned electrocatalytic production of H_2 from H_2O – require particular demands for their synthesis and spectroscopic characterization.[5,20–29] Accordingly, the number of such complexes is comparably limited and insight into the understanding of the intrinsic bonding situation is still lacking behind their uranyl analogues. Consequently, compounds featuring uranium–oxygen bonds in the form of oxidos[18,20,29–43] or hydroxidos[10–16,18] are of particular interest, due to the varying degree of multiple bonding character in the U–O bonds and their resulting reactivity. In combination with a strictly retained ligand environment, essential information about the molecular and electronic structure of these U–O/OH species can be obtained. However, pairs of uranium oxido/hydroxido complexes – supported by an identical ligand system – remain exceedingly rare.

Here, we present the preparation, characterization, and redox-behavior of two uranium(IV/V) and uranium(IV/V/VI) hydroxido/oxido pairs, and closely related fluorido complexes, utilizing a low-valent uranium center surrounded by a newly developed chelate, the cyclen-anchored tris-aryloxide ligand precursor 1,4,7-tris-(3,5-di-*tert*-butyl-2-hydroxy-benzyl)-10-methyl-1,4,7,10-tetraazacyclododecane, abbreviated as cyclen(Me)($^{t\text{-Bu},t\text{-Bu}}$ArOH)$_3$ (Scheme 1, left).

Results and discussion

The new seven-coordinate tris-aryloxide ligand precursor, cyclen(Me)($^{t\text{-Bu},t\text{-Bu}}$ArOH)$_3$, represents a variation of the literature-known, cyclen-anchored, eight-coordinate tetrakis-aryloxide (cyclen($^{t\text{-Bu},t\text{-Bu}}$ArOH)$_4$) (Scheme 1). The corresponding U(IV) complex, [U^{IV}((OAr$^{t\text{-Bu},t\text{-Bu}}$)$_4$cyclen)], possesses a remarkable stability with accompanied low reactivity towards small molecules; most notably, including H_2O.[44] Cyclen-anchored tetrakis-aryloxide chelates of the type cyclen(^{R1,R2}ArO)$_4$ (with R_1 = Me, *t*-Bu; R_2 = Me) were first coordinated to terbium.[45,46] To increase their metal complexes' reactivity and enable the capability of small molecule activation, one aryloxide arm is substituted by a methyl (Me) group. This opens up coordination sites in axial and equatorial positions and engenders the formation of a more reactive trivalent precursor after complexation to uranium. For this purpose, the cyclen-derived anchoring unit 1-methyl-1,4,7,10-tetraazacyclododecane (methyl-cyclen) was synthesized by a modest variation of a literature-known procedure, adopted from Rodríguez–Rodríguez *et al.*[47] A subsequent S_N2-reaction with 2-bromomethyl-4,6-di-*t*-butylphenol as the electrophile yields the ligand precursor (1,4,7-tris-(3,5-di-*tert*-butyl-2-hydroxy-benzyl)-10-methyl-1,4,7,10-tetraazacyclododecane) (($^{t\text{-Bu},t\text{-Bu}}$ArOH)$_3$(Me)cyclen; yield: 93%).

Reaction of cyclen(Me)($^{t\text{-Bu},t\text{-Bu}}$ArOH)$_3$ with [U^{III}(N(SiMe$_3$)$_2$)$_3$][48] in thawing benzene generates the target precursor complex [U^{III}((OAr$^{t\text{-Bu},t\text{-Bu}}$)$_3$(Me)cyclen)] (**1**) in 65% yield (Scheme 1). ^{1}H NMR analysis of **1** in benzene-d_6 shows 12 of the 15 signals for the 85 hydrogen atoms, paramagnetically broadened and shifted, in the range from 15.17 to −13.29 ppm (Fig. S6†). The number of signals suggests C_S symmetry in solution and the lack of some signals can be explained by strong broadening due to the coordination of the chelate to the paramagnetic U(III) f^3 ion. The bulk purity of **1** was established by CHN combustion analysis, and its 3+ oxidation state is unambiguously supported by UV/vis/NIR electronic absorption spectroscopy (Fig. 3, top) and SQUID magnetic measurements (Fig. S47–S49†). We assume that the ligand's high flexibility prevents the formation of suitable single-crystals for X-ray diffraction (SC-XRD) analysis. Although the structural proof of **1** is missing, all characterizations, the subsequent reactivity, and structural studies support the formation and existence of the targeted uranium(III) precursor complex. For instance, oxidation of **1** with a few drops of methylene chloride yields the corresponding uranium(IV) complex, [(cyclen(Me)($^{t\text{-Bu},t\text{-Bu}}$ArO)$_3$)U^{IV}(Cl)] (**2**) (Scheme 1, 76% yield). For **2**, suitable single-crystals for SC-XRD analysis were obtained by slow diffusion of pentane into a concentrated THF solution (**2** × **2** THF),

 © 2022 The Author(s). Published by the Royal Society of Chemistry

Open Access Article. Published on 12 August 2022. Downloaded on 1/22/2026 11:04:29 AM.
This article is licensed under a Creative Commons Attribution-NonCommercial 3.0 Unported Licence.

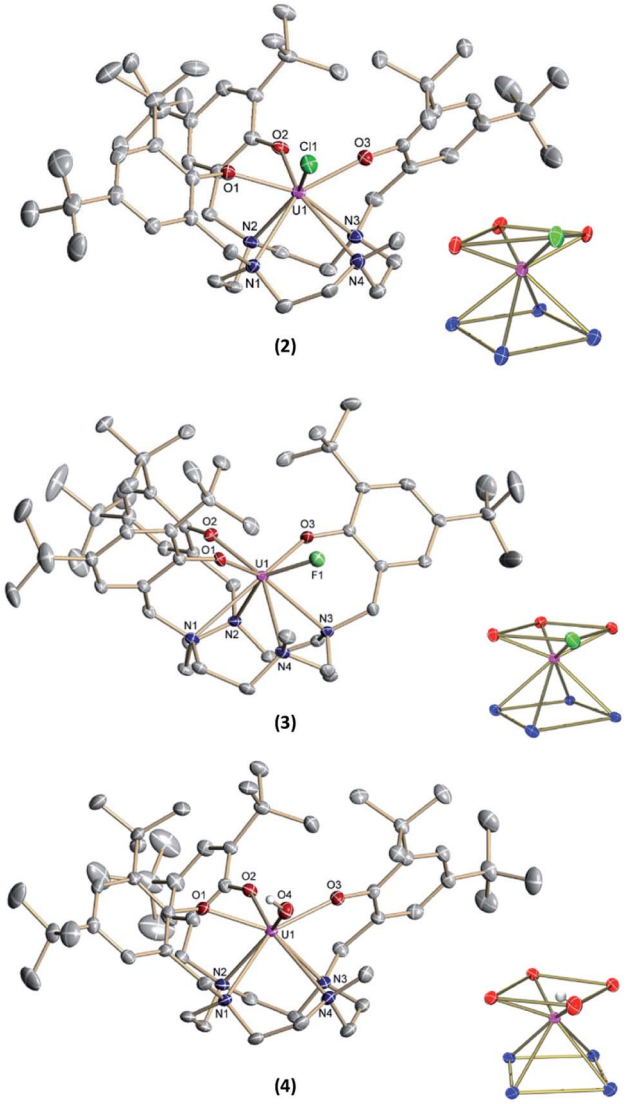

Fig. 1 Solid-state molecular structures of **2** (top), **3** (middle), and **4** (bottom) in crystals of $[(cyclen(Me)(^{t\text{-}Bu,t\text{-}Bu}ArO)_3)U^{IV}(Cl)] \times 2.5$ benzene, $[(cyclen(Me)(^{t\text{-}Bu,t\text{-}Bu}ArO)_3)U^{IV}(F)] \times 2\ Et_2O$, and $[(cyclen(Me)(^{t\text{-}Bu,t\text{-}Bu}ArO)_3)U^{IV}(OH)] \times 2$ THF, respectively, as well as the coordination polyhedra of the heteroatoms (each bottom right). Hydrogen atoms (except for the hydroxyl H), co-crystallized solvent molecules, and the second component (**3**) in the mixed crystal are omitted for clarity. Thermal ellipsoids are shown at the 50% probability level.

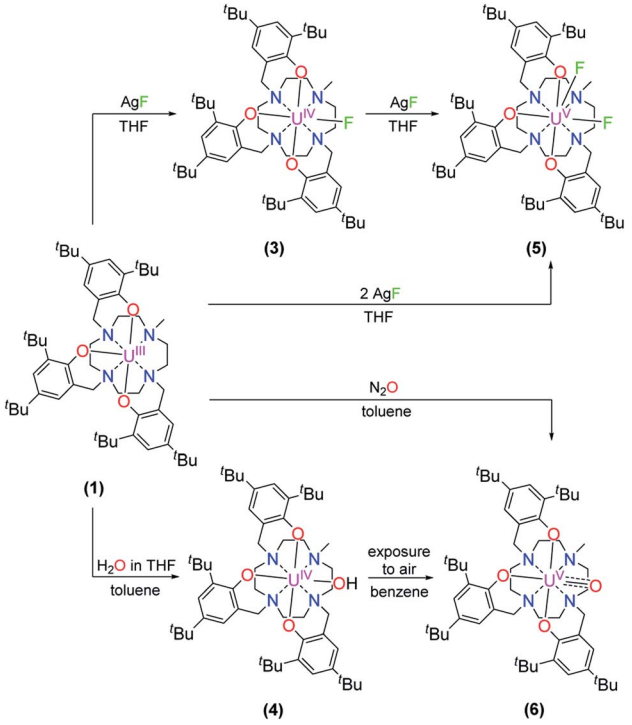

Scheme 2 Synthesis of $[(cyclen(Me)(^{t\text{-}Bu,t\text{-}Bu}ArO)_3)U^{IV}(F)]$ (**3**), $[(cyclen(Me)(^{t\text{-}Bu,t\text{-}Bu}ArO)_3)U^{IV}(OH)]$ (**4**), $[(cyclen(Me)(^{t\text{-}Bu,t\text{-}Bu}ArO)_3)U^{V}(F)_2]$ (**5**), and $[(cyclen(Me)(^{t\text{-}Bu,t\text{-}Bu}ArO)_3)U^{V}(O)]$ (**6**).

which crystallizes in the orthorhombic space group $P2_12_12_1$. Better quality crystals of **2** were obtained from a concentrated benzene solution, which crystallized in the monoclinic space group $P2_1/n$. The molecular structures observed in the two determined crystal structures are very similar and only the latter (**2** × 2.5 benzene) will be discussed here (Fig. 1, top; Table 1). Tetravalent **2** reveals a distorted square antiprismatic geometry with an N_4O_3Cl polyhedron, consisting of the cyclen's N_4 and an O_3Cl plane. Notably, the chloride ligand is not coordinated in an axial position but with a slight shift of 0.628 Å out of the plane of the three aryloxide ligands and with a dihedral angle of 47.2(3)° to the substituted cyclic amine's methyl group. The U–Cl bond distance is 2.734(1) Å and the average $U\text{–}O_{ArO}$ (2.179(3) Å) and $U\text{–}N_{cyclen}$ (2.732(4) Å) distances are in agreement with literature values of the cyclen- and tacn-based U(IV) complexes $[U(OAr^{t\text{-}Bu,t\text{-}Bu})_4cyclen)]$[44] and $[(tacn(^{R,R'}ArO)_3)U^{IV}(Cl)]$ (R = *t*Amyl, DMB, Ad, neoP, *t*-Bu, Dia; R′ = *t*Amyl, DMB, *t*-Bu, Me) (Cl, axially bound, d(U–Cl) = 2.691(3)–2.875(5) Å).[49–52]

Treatment of $[(cyclen(Me)(^{t\text{-}Bu,t\text{-}Bu}ArO)_3)U^{III}]$ (**1**) with stoichiometric amounts of AgF induces a one-electron oxidation and leads to the formation of $[(cyclen(Me)(^{t\text{-}Bu,t\text{-}Bu}ArO)_3)U(F)]$ (**3**) in 36% yield with concomitant precipitation of elemental silver. Similarly, oxidation of **1** with a slight excess of H_2O (0.2 M solution in THF) results in the corresponding U(IV) hydroxido derivative $[(cyclen(Me)(^{t\text{-}Bu,t\text{-}Bu}ArO)_3)U^{IV}(OH)]$ (**4**) in 23% yield (Scheme 2). ^1H NMR spectroscopy reveals signals ranging from 60.78 to −65.59 ppm for **3** and 64.76 to −67.77 ppm for **4**, respectively (Fig. S8 and S9†). As expected, the spectra of **3** and **4** are quite comparable and show the 35 signals originating from the 85 and 86 protons, respectively. This is in accordance with the expected C_S symmetry in the solution. While the acidic OH proton of **4** has not been observed and likely is broadened into the baseline by rapid exchange or paramagnetism, the six most dominant peaks at 4.88, 4.04, 3.83, −6.52, −9.65 and −12.35 ppm for **3** and 5.16, 5.00, 3.82, −3.16, −12.26 and −13.35 ppm for **4** can be assigned to the *t*-butyl groups. Moreover, the methyl groups can be detected at 33.21 ppm for **3** and 20.14 ppm for **4**. The OH group of **4** was detected *via* infrared vibrational spectroscopy centered at a wavenumber $\tilde{\nu}$ of 3675 cm^{-1}.

Open Access Article. Published on 12 August 2022. Downloaded on 1/22/2026 11:04:29 AM.
This article is licensed under a Creative Commons Attribution-NonCommercial 3.0 Unported Licence.

Table 1 Selected bond lengths (Å) for complexes **2**, **3**, **4**, **5**, and **6**, together with the literature-known [(cyclen($^{t\text{-Bu},t\text{-Bu}}$ArO)$_4$)U][44] for comparison

	2 × 2 THF	**2** × 2.5 benzene	**3**	**4**	**5**	**6**	[(cyclen($^{t\text{-Bu},t\text{-Bu}}$ArO)$_4$)U]
U–O1$_{ArO}$	2.152(6)	2.195(3)	2.176(2)	2.231(2)	2.123(2)	2.234(3)	2.203(2)
U–O2$_{ArO}$	2.211(6)	2.173(2)	2.213(2)	2.233(2)	2.096(2)	2.183(3)	2.228(2)
U–O3$_{ArO}$	2.175(6)	2.170(3)	2.196(2)	2.208(2)	2.137(2)	2.211(4)	2.203(2)
U–O4$_{ArO}$	—	—	—	—	—	—	2.228(2)
U–O$_{ArO}$ (av)	2.179(6)	2.179(3)	2.195(2)	2.224(2)	2.119(2)	2.209(6)	2.216(2)
U–N1	2.717(8)	2.715(3)	2.770(2)	2.730(2)	2.895(3)	2.688(4)	2.801(2)
U–N2	2.675(7)	2.708(3)	2.778(2)	2.784(3)	2.851(3)	2.759(4)	2.755(2)
U–N3	2.765(8)	2.772(3)	2.708(2)	2.817(2)	2.983(3)	2.850(4)	2.801(2)
U–N4	2.788(8)	2.810(3)	2.805(2)	2.817(3)	3.018(3)	2.743(4)	2.755(2)
U–N$_{cyclen}$ (av)	2.736(8)	2.751(3)	2.765(2)	2.787(3)	2.937(3)	2.760(4)	2.778(2)
U$_{oop}$	−0.949(3)	−0.952(2)	−0.875(5)	−0.865(1)	−0.480(2)	−0.801(2)	−0.879(2)
U–L$_{eq}$	2.770(2)	2.734(1)	2.118(1)	2.141(2)	2.106(2)	1.850(3)	—
U–L$_{ax}$	—	—	—	—	2.105(2)	—	—

Suitable single-crystals of complexes **3** and **4** were grown from a concentrated THF solution and slow evaporation of a saturated THF solution, respectively (Fig. 1). Both complexes crystallize in monoclinic space groups, namely $P2_1/c$ (**3**) and $P2_1/n$ (**4**). The U–X (X = F (**3**) and OH (**4**)) bond distances are 2.118(2) Å and 2.141(2) Å, respectively. Notably, in the crystal structure of **4**, the position of the O4 bound hydrogen atom H4 has been unequivocally identified in a difference Fourier map. The correctness of the determined H4 position is further supported by the involvement of this O–H group in a hydrogen bond to the oxygen atom of one of the located solvent tetrahydrofuran molecules (for details see ESI†). The average U–O$_{ArO}$ und U–N$_{cyclen}$ distances are in agreement with literature-reported values of the cyclen- and tacn-based U(IV) complexes [(cyclen($^{t\text{-Bu},t\text{-Bu}}$ArO)$_4$)U] and [(tacn($^{R,R'}$ArO)$_3$)U^{IV}(X)] (X = axially bound ligand) (Table 1). Both molecules reveal a distorted square antiprism-like geometry with an N$_4$O$_3$X polyhedron scaffold consisting of an N$_4$ and an O$_3$X plane. Thereby, the fluorido and hydroxido ligand fit well into the vacant site of the O$_3$X plane with out-of-plane shifts of 0.040(3) Å for **3** and 0.165(5) Å for **4**. Tetravalent **3** is conveniently oxidized with silver fluoride to yield the corresponding U(V) complex [(cyclen(Me)($^{t\text{-Bu},t\text{-Bu}}$ArO)$_3$)U^{V}(F)$_2$] (**5**) in 23% yield (Scheme 2). Compound **5** is also accessible by treating **1** with two equivalents of AgF. Suitable single crystals of **5** were obtained from slow diffusion of *n*-pentane into a concentrated Et$_2$O solution at −30 °C, but always in the form of mixed crystals with an approximate ratio of 80 : 20% of the components [(cyclen(Me)-($^{t\text{-Bu},t\text{-Bu}}$ArO)$_3$)U^{V}(F)$_2$] (**5**) (Fig. 2, top) and [(cyclen(Me)-($^{t\text{-Bu},t\text{-Bu}}$ArO)$_3$)U^{IV}(F)] (**3**). The compound crystallizes in the monoclinic space group $P2_1/n$, revealing the expected *cis* orientation of the two fluorido ligands for **5**. The geometry of the complex is best described as capped, distorted square antiprismatic, with one fluorido ligand in the equatorial O$_3$F$_{eq}$ plane and one axial fluorido ligand (F$_{ax}$). The occupation of the axial position forces F$_{eq}$ to shift towards the cyclen methyl group. The resulting repulsion leads to a slightly longer U–N$_4$ distance (3.018(3) Å with regard to complex **3** (2.805(2) Å). Complex **5** demonstrates that it is, in principle, possible to bind a ninth, axial ligand in *cis*-position to a monodentate equatorial ligand. This is an important prerequisite in water reduction catalysis, where a *cis*-hydroxido/hydrido intermediate is an imperative intermediate in the postulated reaction mechanism.[20]

The ^{1}H NMR spectra of the U(V) complex **5** shows 26 resonances that range from 17.08 to −5.94 ppm (Fig. S10†). The spectrum shows a pattern consisting of six resonances in the aromatic region (10.51 to 8.04 ppm), one broad signal (5.94 ppm), two nearby sharp singlets (4.49 and 4.31 ppm), a broad

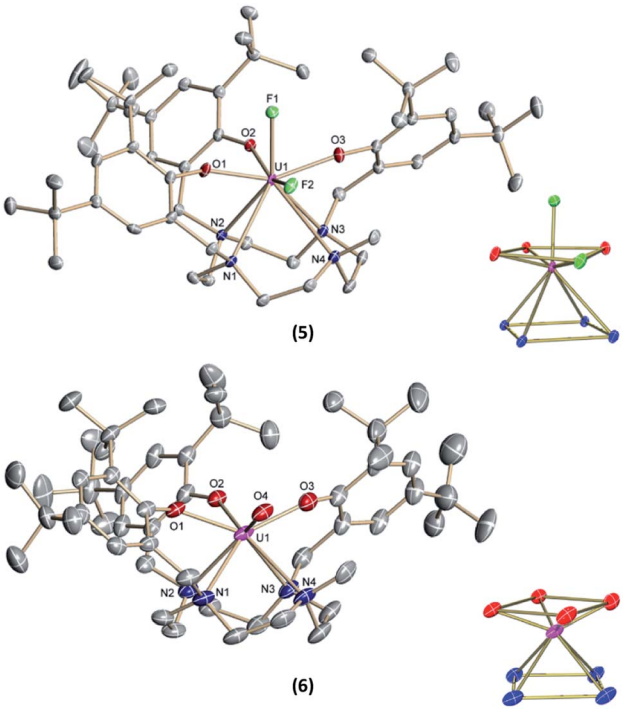

Fig. 2 Solid-state molecular structures of **5** (top) and **6** (bottom) in crystals of [(cyclen(Me)($^{t\text{-Bu},t\text{-Bu}}$ArO)$_3$)U^{V}(F)$_2$]$_{0.8}$[(cyclen(Me)-($^{t\text{-Bu},t\text{-Bu}}$ArO)$_3$)U^{IV}(F)]$_{0.2}$ × 2 Et$_2$O and [(cyclen(Me)($^{t\text{-Bu},t\text{-Bu}}$ArO)$_3$)U^{V}(O)] × 1.5 THF, respectively, as well as the coordination polyhedra of the heteroatoms (each bottom right). Hydrogen atoms and co-crystallized solvent molecules are omitted for clarity. Thermal ellipsoids are shown at the 50% probability level.

 © 2022 The Author(s). Published by the Royal Society of Chemistry

Open Access Article. Published on 12 August 2022. Downloaded on 1/22/2026 11:04:29 AM.
This article is licensed under a Creative Commons Attribution-NonCommercial 3.0 Unported Licence.

singlet (2.04 ppm), three nearby sharp singlets (1.87, 1.79 and 1.70 ppm) and two further broad singlets (0.30 and −0.39 ppm).

Complex **1** also serves as a starting material for the oxido complex [(cyclen(Me)($^{t\text{-Bu},t\text{-Bu}}$ArO)$_3$U^{V}(O)] (**6**) when treating the precursor with oxygen-atom transfer (OAT) reagents, such as N_2O gas, 2,2,6,6-tetramethylpiperidinyloxyl (TEMPO) or trimethylamine *N*-oxide (Me_3NO). Remarkably, pentavalent oxido **6** is also formed when a benzene solution of hydroxido **4** is exposed to air for several days. Regardless, the highest yield (61%) of **6** was accomplished by stirring **1** under an atmosphere of N_2O in toluene solution overnight (Scheme 2).

Single-crystals suitable for SC-XRD analysis of **6** were obtained by slow evaporation of a concentrated THF solution at −30 °C (Fig. 2, bottom). Complex **6** crystallizes in the monoclinic space group *C*2/*c*. Despite the different oxidation states of the uranium center, the geometry, structure, and bond lengths of **6** are comparable to the U(IV) fluorido and hydroxido complexes **3** and **4**, the main difference being the short U(V)–O bond distance of 1.850(3) Å. While the U═O bond length in **6** is in agreement with literature-known values for terminal U(V) oxo complexes (1.706–1.863 Å),[11–18,45] it is noteworthy that the oxido atom is situated perfectly within the O_3X plane and that the oxido's equatorial binding mode is quite uncommon, with merely two other comparable examples reported in the literature; namely, the tacn-based neo-pentyl-substituted complexes [(tacn(^{nP,Me}ArO)$_3$)U^{V}(O)(X)] (X = O–Py, O–NMe$_3$). In the latter cases, the axial position is occupied by the donor ligands pyridine *N*-oxide or trimethylamine-*N*-oxide. In **6**, however, the axial coordination site remains open. One possible reason for the preferred equatorial binding mode could be the inverse trans influence (ITI).[19,53–56] Although the ∢ O4–U1–O2 angle is significantly bent (132.8(2) °), the ITI is reflected in the shorter uranium – aryloxide U–O2 bond distance (2.183(3) Å) *trans* to the oxido ligand. This bond is about 0.04 Å shorter than the U–O_{Ar} bonds in *cis* position (U–O1 = 2.234(3) Å and U–O3 = 2.211(4) Å). In this context, it is also worth mentioning that the U–O2 bond distances *trans* to the bound chlorido ligand in **2** (2.211(6) Å) and the fluorido ligand in **3** (2.213(1) Å) are slightly longer than the U–O1 and U–O3 bond distances (2.152(6) and 2.175(6) Å for **2**, 2.176(1) and 2.196(1) Å for **3**). This observation suggests a stronger ITI of the aryloxides than of the chloride and fluoride, which is in agreement with the literature.[19] The fact that the newly employed, low-symmetry seven-coordinate chelate, plus the additional oxido/hydroxido ligands, enforce a geometry with four oxygen donors on one face and four nitrogen donors on the other, allows for a comparison of uranium complexes with our group's "classic" tris-aryloxide-tacn-based systems (N_3O_3) and a number of extended solids, including those with $[UO_2]^{2+}$ motifs.

Electronic absorption spectroscopy

The electronic absorption spectra of complexes **1**, **2**, **3**, and **4** (Fig. 3) clearly reflect the difference between the uranium(III) and the uranium(IV) oxidation states. In uranium(III) complexes, the 5f–6d energy gap is smaller than in uranium(IV) complexes. As a consequence, the Laporte-allowed 5f–6d transitions are shifted towards lower energy, *viz.* higher wavelength, for uranium(III), usually between 500–700 nm.[57] Consequently, these chromophoric transitions of dark purple **1** are located at 537 nm (ε = 1220 M^{-1} cm^{-1}), 515 nm (ε = 1215 M^{-1} cm^{-1}), and 465 nm (ε = 1180 M^{-1} cm^{-1}) and the pale green color of complexes **2**, **3** and **4** seems to originate from absorption bands centered at 325 nm (ε

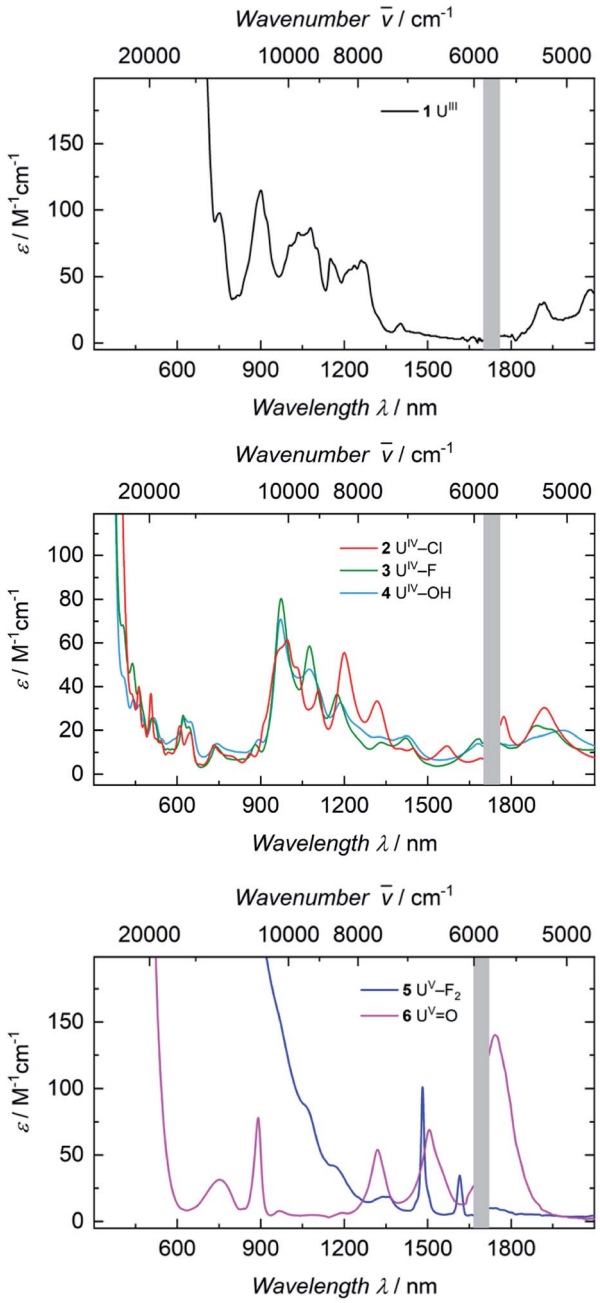

Fig. 3 Top: Electronic absorption spectrum of complex **1** recorded at room temperature in benzene solution. Middle: Electronic absorption spectra of complexes **2**, **3** and **4** recorded at room temperature in THF solution. Bottom: Electronic absorption spectra of complexes **5** and **6** recorded at room temperature in benzene solution (**5**) and THF solution (**6**). Data points from 1700 nm to 1760 nm (top and middle) and 1660 nm to 1720 nm (bottom) are omitted due to the change from a PbS to an In/Ga/As detector.

Open Access Article. Published on 12 August 2022. Downloaded on 1/22/2026 11:04:29 AM.
This article is licensed under a Creative Commons Attribution-NonCommercial 3.0 Unported Licence.

= 8000 M^{-1} cm^{-1} for **2**, ε = 6000 M^{-1} cm^{-1} for **3**, ε = 4500 M^{-1} cm^{-1} for **4**, see SI), starting to gain intensity from 400 nm (Fig. 3). The UV region of uranium(IV) complexes is characteristic for charge-transfer bands, likely originating from ligand-based $\pi \rightarrow \pi^*$, LMCT or MLCT and inter-configurational 5f–6d transitions.[58] All further low-intensity absorption bands in the range from 400 to 2100 nm arise from Laporte-forbidden f–f transitions and, therefore, exhibit small extinction coefficients of $\varepsilon \approx$ 10–60 M^{-1} cm^{-1} for **2**, 10–77 M^{-1} cm^{-1} for **3**, and 10–64 M^{-1} cm^{-1} for **4** (Fig. 3, middle). The number and shape of the bands of **2**, **3** and **4** is in accordance with the typical pattern observed for the $5f^2$ electronic configuration of uranium(IV) complexes.[45,66,63–65] As expected from the similar molecular structure and geometry, the data for **3** and **4** are very comparable over the whole spectral range, even though the maximum intensities slightly vary (ε = 77 M^{-1} cm^{-1} for **3**, ε = 64 M^{-1} cm^{-1} for **4**).

The dark black color of the U(V) complex **5** can be explained by the intense absorptions starting in the NIR region at 1020 nm (value given for ε = 100 M^{-1} cm^{-1}) (Fig. 3, bottom), covering the entire visible light spectrum. This, in combination with the NIR region that is dominated by only a few, notably sharp Laporte forbidden f–f transitions, is in agreement with a U(V) metal center with its $5f^1$ electronic configuration and resulting $^2F_{5/2}$ ground state with seven non-degenerate energetic states for both complexes (Fig. 4).[2,43] As a consequence, only six f–f transitions are possible in U(V) complexes. For **5**, two sharp (1480 and 1615 nm) and four broad transitions (1065 nm, 1160 nm and 1735 nm) are detected with the most intense band located at 1480 nm with ε = 98 M^{-1} cm^{-1}. The strong absorption band of **6** starts at 527 nm in the visible region, explaining the bright orange color of this compound. This hypsochromic shift of the assumed 5f–6d transitions simplifies the detection of five f–f transitions in the case of **6**. The transitions are detected at 760 nm (ε = 27 M^{-1} cm^{-1}), 890 nm (ε = 65 M^{-1} cm^{-1}), 1322 nm (ε = 46 M^{-1} cm^{-1}), 1507 nm (ε = 59 M^{-1} cm^{-1}), and 1760 nm (ε = 105 M^{-1} cm^{-1}) (Fig. 3, bottom). The transitions of **5** are weaker than those of **6**, presumably due to greater orbital mixing in the latter.

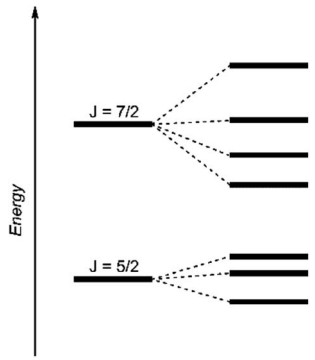

Fig. 4 Schematic energy levels for a $5f^1$ system assuming the spin–orbit interaction is greater than the ligand field interaction.[29]

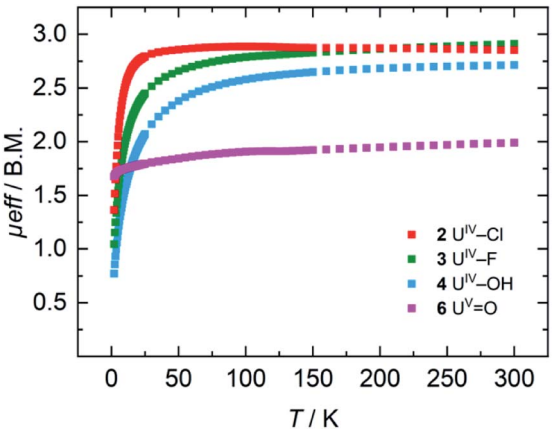

Fig. 5 VT SQUID magnetization measurements of microcrystalline, solid samples of **2**, **3**, **4**, and **6**. The plot shows averaged values of two independently synthesized samples.

Magnetism

For the tetravalent complexes, variable temperature-dependent SQUID measurements reveal an effective magnetic moment, μ_{eff}, of 1.36 μ_B at 2 K and 2.81 μ_B at 300 K for the chlorido complex **2**, 1.04 μ_B at 2 K and 2.91 μ_B at 300 K for fluorido **3**, and 0.77 μ_B at 2 K and 2.72 μ_B at 300 K for hydroxido **4** (Fig. 5). Especially the low-temperature magnetic moment of **2** is relatively high for uranium(IV) complexes with its $5f^2$ electronic configuration and its, presumably, $^3H_4$ non-magnetic ground state,[59] suggests either a high contribution of temperature-independent paramagnetism (TIP) at low temperatures or an unusual pseudo-doublet ground state.[60,61] Tetravalent complexes of the tacn-based tris-aryloxide ligand system, for instance, often possess low-temperature moments down to approx. 0.3 μ_B.[52] In the case of **3** and **4**, the magnetic data is comparable to that of $[U^{IV}((OAr^{t\text{-}Bu,t\text{-}Bu})_4cyclen)]$.[44]

Pentavalent **6** is nearly temperature-independent with a low-temperature value of μ_{eff} = 1.68 μ_B at 2 K, which increases to 1.99 μ_B at 300 K. This behavior is ordinary for a U(V) ion with a $5f^1$ electronic configuration and a $^2F_{5/2}$ ground state.[67] Furthermore, the magnetic data of **6** compare well with that of the tacn-based oxido complex $[(tacn(^{t\text{-}Bu}ArO)_3)U^V(O)]$ (1.61 μ_B at 5 K, and 1.98 μ_B at 300 K), despite the fact that the oxido ligand is bound in the axial position for $[(tacn(^{t\text{-}Bu}ArO)_3)U^V(O)]$.[29] Interestingly, the tacn-based and neo-pentyl-substituted systems $[(tacn(^{nP,Me}ArO)_3)U^V(O)(X)]$ (X = O–Py, O–NMe_3), with the oxido ligand coordinated in the equatorial site and an additional neutral donor ligand in the axial site, show a strikingly different magnetic behavior.[64] This leads to the assumption that the addition of another (neutral) ligand and, thus, a change from an 8-coordinated to a 9-coordinated complex, has a stronger influence on the magnetic properties than a change of the oxido ligand from an axial to an equatorial position.

Electrochemistry

Cyclic voltammetry studies of complexes **1**, **2**, **3**, and **4** all show two major reversible redox-events for each complex (see SI). For

 © 2022 The Author(s). Published by the Royal Society of Chemistry

Open Access Article. Published on 12 August 2022. Downloaded on 1/22/2026 11:04:29 AM.
This article is licensed under a Creative Commons Attribution-NonCommercial 3.0 Unported Licence.

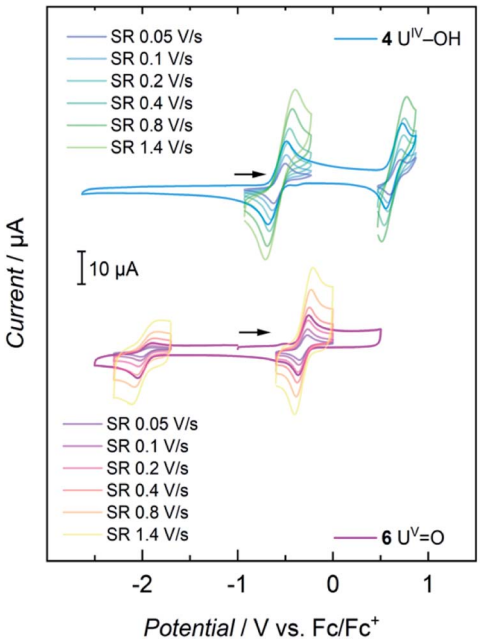

Fig. 6 Cyclic voltammograms of **4** and **6** at scan rates varying from 0.05 to 1.4 V s^{-1}, recorded in THF solution with 0.1 M $TBAPF_6$ as supporting electrolyte.

1, the events at a half-wave potential of $E_{1/2} = -1.71$ V (all values referenced to $[FeCp_2]^{0/+}$ at 0.0 V) and at $E_{1/2} = 0.00$ V can be attributed to the U(III/IV) and U(IV/V) redox couples according to linear sweep measurements. Accordingly, **1** is quite sensitive to electrolysis and decomposes to a U(IV) species over the course of several measurements. The main reversible redox events of **2**, **3** and **4** occur at half-wave potentials of $E_{1/2} = 0.12$ V, $E_{1/2} = -0.12$ V and $E_{1/2} = -0.59$ V for the U(IV/V) couples, and $E_{1/2} = 0.85$ V, $E_{1/2} = 1.06$ V and $E_{1/2} = 0.64$ V for the U(V/VI) couple, respectively (see SI). The cyclic voltammogram of **6** shows one non-reversible redox event at $E_{1/2} = -1.97$ V and one reversible at $E_{1/2} = -0.32$ V. The more negative one probably accounts for the reduction to a U(IV) species when scanning in a cathodic direction. According to linear sweep measurements, the event at $E_{1/2} = -0.32$ V can be assigned to the U(V/VI) redox couple. The metal-centered oxidations of hydroxido **4** and oxido **6** (Fig. 6) are of particular interest and, indeed, it was possible to chemically oxidize these complexes while retaining their structural main features (*vide infra*).

Redox chemistry of [(cyclen(Me)($^{t\text{-Bu},t\text{-Bu}}$ArO)$_3$)U^{IV}(OH)] and [(cyclen(Me)($^{t\text{-Bu},t\text{-Bu}}$ArO)$_3$)U^{V}(O)]

Accordingly, one-electron oxidation of **4** and **6** with $AgSbF_6$ yields the corresponding U(V) and U(VI) complexes [(cyclen(Me)($^{t\text{-Bu},t\text{-Bu}}$ArO)$_3$)U^{V}(OH)][$SbF_6$] (**7**) and [(cyclen(Me)($^{t\text{-Bu},t\text{-Bu}}$ArO)$_3$)U^{VI}(O)][$SbF_6$] (**8**) in 80% and 39% yield, respectively (Scheme 3).

The ^{1}H NMR spectrum of **7** shows a paramagnetic influence of the uranium(V) center with the resonances ranging from 36.04 to −25.41 ppm (Fig. S12†). By integration, the *t*-butyl groups can readily be attributed to the resonances at 4.48, 4.42, 1.04, −2.39, −4.75 and −4.85 ppm. The ^{1}H NMR spectrum of **8**

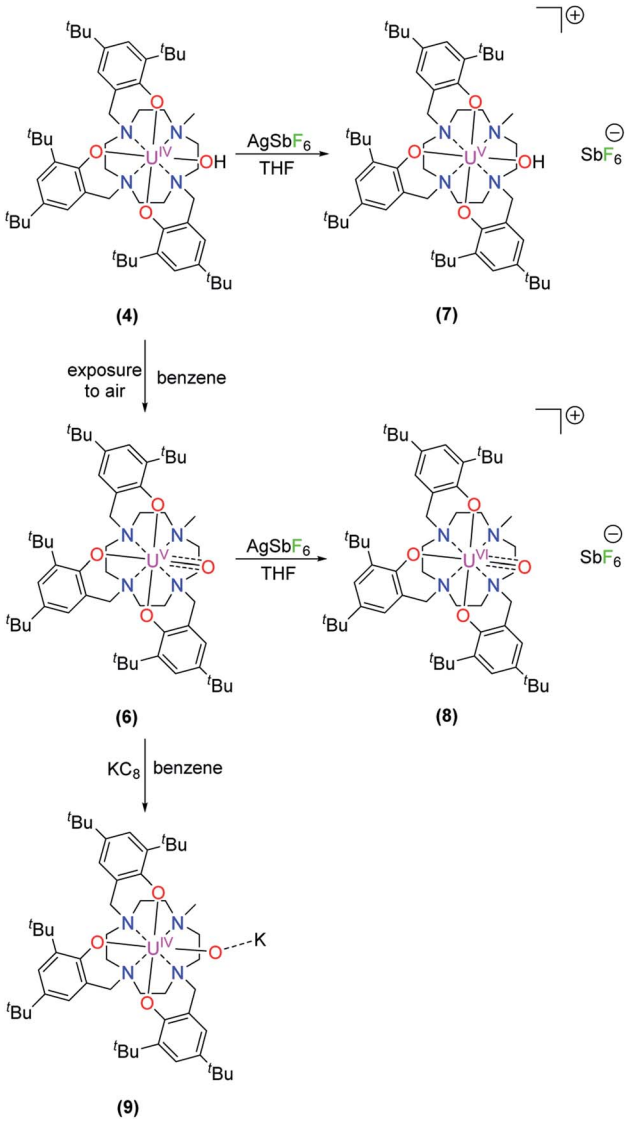

Scheme 3 Synthesis of [(cyclen(Me)($^{t\text{-Bu},t\text{-Bu}}$ArO)$_3$)U^{V}(OH)][$SbF_6$] (**7**), [(cyclen(Me)($^{t\text{-Bu},t\text{-Bu}}$ArO)$_3$)U^{VI}(O)][$SbF_6$] (**8**), and K[(cyclen(Me)($^{t\text{-Bu},t\text{-Bu}}$ArO)$_3$)U^{IV}(O)] (**9**).

instead is characteristic for a uranium(VI) center with resonances in deuterated benzene in the diamagnetic region ranging from 8.11 to 1.12 ppm, with the resonances of the *t*-butyl groups at 1.80, 1.48, 1.43, 1.32 and 1.16 ppm, where the signal at 1.32 ppm accounts for two *t*-butyl groups according to the integration. Due to paramagnetic resonances in spectra of diamagnetic **8**, even after crystallization, VT-VF ^{1}H NMR studies were performed (see SI). The analyses suggest that the observed paramagnetic signals stem from trace amounts of **7** (*ca.* 3%) rather than magnetic excited states/TIP of **8**.

Single-crystals suitable for SC-XRD analysis for **7** and **8** (Fig. 7) were grown from concentrated benzene solutions. Both complexes crystallize in the monoclinic space group *P*2/*c*. Due to the higher oxidation states of the uranium centers, the average U–O_{ArO} and U–N_{cyclen} bond distances decrease from 2.224(2) Å and 2.787(3) Å in **4** to 2.113(2) Å and 2.691(3) Å in **7**

Open Access Article. Published on 12 August 2022. Downloaded on 1/22/2026 11:04:29 AM.
This article is licensed under a Creative Commons Attribution-NonCommercial 3.0 Unported Licence.

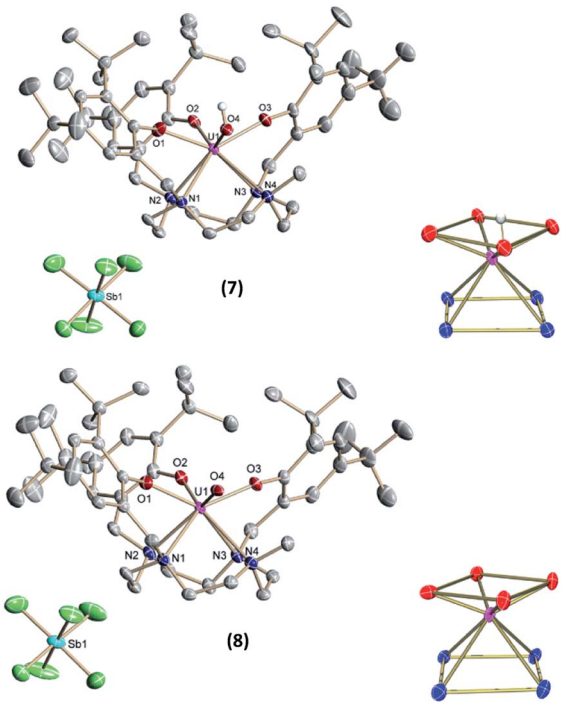

Fig. 7 Solid-state molecular structure of **7** (top) and **8** (bottom) in crystals of $[(cyclen(Me)(^{t\text{-}Bu,t\text{-}Bu}ArO)_3)U^{V}(OH)][SbF_6] \times 3.5$ benzene and $[(cyclen(Me)(^{t\text{-}Bu,t\text{-}Bu}ArO)_3)U^{VI}(O)][SbF_6] \times 3.5$ benzene, as well as the coordination polyhedra of the heteroatoms (bottom right). Hydrogen atoms (except for the hydroxido H) and co-crystallized solvent molecules are omitted for clarity. Thermal ellipsoids are shown at the 50% probability level.

and from 2.179(6) and 2.760(4) in **6** to 2.116(2) and 2.698(3) in **8**. Also, the U–OH bond distance decreases slightly from 2.141(2) Å in **4** to 2.052(2) Å in **7** (Table 2). It should be noted that in the crystal structure of **7** the position of the O4 bound hydrogen atom H4 could not be unequivocally derived from a difference Fourier synthesis. We have decided to use the O4 bound hydrogen atom in a calculated position and subsequently allowed it to ride on its carrier oxygen atom. Evidence for the presence of the hydroxyl group comes from the fact that the unit cell volume of **7** × 3.5 benzene is by 24.5 Å^3 significantly larger than that of the oxido analogue **8** × 3.5 benzene, which crystallizes isostructurally to the hydroxido compound **7**.

Table 2 Selected bond lengths (Å) for complexes **4**, **6**, **7**, and **8**

	4	**6**	**7**	**8**
U–O1	2.231(2)	2.234(3)	2.108(2)	2.119(2)
U–O2	2.233(2)	2.183(3)	2.131(2)	2.123(2)
U–O3	2.208(2)	2.211(4)	2.100(2)	2.106(2)
$U–O_{ArO}$(av)	2.224(2)	2.179(6)	2.113(2)	2.116(2)
U–N1	2.730(2)	2.688(4)	2.646(2)	2.643(3)
U–N2	2.784(3)	2.759(4)	2.652(2)	2.662(3)
U–N3	2.817(2)	2.850(4)	2.706(2)	2.729(3)
U–N4	2.817(3)	2.743(4)	2.759(3)	2.759(3)
$U–N_{cyclen}$(av)	2.787(3)	2.760(4)	2.691(3)	2.698(3)
U_{oop}	−0.865(1)	−0.801(2)	−0.831(1)	−0.804(2)
$U–L_{eq}$(O4)	2.141 (2)	1.850(3)	2.052(2)	1.949(3)

Additionally, the U–O4 (hydroxido) bond distance in **7** × 3.5 benzene of 2.052(2) Å is significantly longer than the U–O4 (oxido) bond distance in **8** × 3.5 benzene of 1.949(3) Å (for further details see SI). Interestingly, the U=O bond is elongated when going from pentavalent **6** (1.850(3) Å) to hexavalent **8** (1.949(3) Å), and is longer than the average bond length of U(VI) non-uranyl U=O complexes, but still within the literature reported range (dU–O = 1.764(5)–1.98(3) Å).[30,35,56,64–68] While we cannot rule out possible contamination of oxido complex **8** with minor impurities of the hydroxido **7** (*vide supra*), we were unable to detect these from the SC-XRD data. In the single-crystal structure determination of **8**, we cannot find additional significant electron density at the location of the oxido ligand. While there is one minor electron density maximum (peak #31 in the list of residual electron density maxima, see ESI) with a height of 0.45 e Å^{-3} that is close to O4 and at a distance of 2.04 Å from the U center, attempts to refine a disorder between an oxido and a hydroxido ligand, including both the original position of O4 and Q31, remained unsuccessful. Eventually, all electron density was always located at the original O4 position.

Finally, treating **6** with KC_8 in benzene solution results in the light green complex **9**, with a yield of 97%, that is identified as

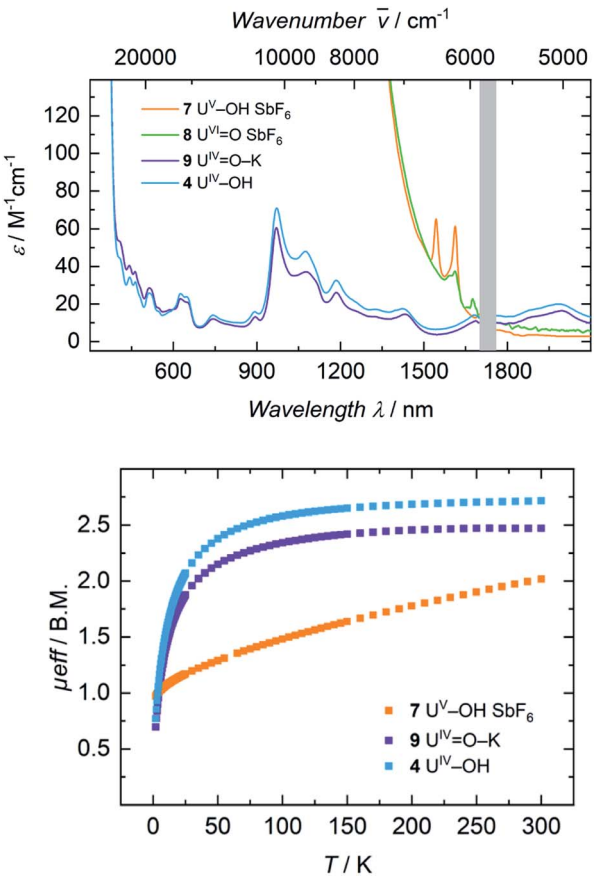

Fig. 8 Top: Electronic absorption spectra of complexes **4**, **7**, **8**, and **9** were recorded at room temperature in benzene (**8**) and THF (**4**, **7**, **9**) solution. Data points from 1700 nm to 1760 nm are omitted due to a detector change from a PbS to an In/Ga/As detector. Bottom: VT SQUID magnetization measurements of microcrystalline, solid samples of **4**, **7** and **9**.

 © 2022 The Author(s). Published by the Royal Society of Chemistry

Open Access Article. Published on 12 August 2022. Downloaded on 1/22/2026 11:04:29 AM.
This article is licensed under a Creative Commons Attribution-NonCommercial 3.0 Unported Licence.

a uranium(IV) species by vis/NIR absorption spectroscopy and SQUID magnetometry (Fig. 8). Even though single-crystals suitable for XRD analysis could not be obtained, especially the electronic absorption measurements suggest that, in THF solution, the molecular structure of **9** is similar to that of hydroxido **4** (Scheme 3 and Fig. 8).

The ^{1}H NMR spectrum of complex **9** shows resonances over a range from 91.50 to −72.47 ppm (Fig. S15†). The six *t*-butyl resonances can be attributed by integration to the signals at 11.93, −2.38, −3.02, −4.33, −9.16 and −20.24 ppm.

Electronic absorption spectra of **7** and **8** feature exceedingly intense absorptions below $\lambda = 1400$ nm ($\varepsilon > 2000$ M^{-1} cm^{-1}), explaining the dark black color of both complexes (Fig. 8, top). Above 1500 nm, the uranium(V) hydroxido **7** reveals two sharp bands at 1545 nm ($\varepsilon = 65$ M^{-1} cm^{-1}) and 1615 nm ($\varepsilon = 60$ M^{-1} cm^{-1}), while the uranium(VI) oxido **8** shows two, very weak absorptions at 1610 nm with a shoulder at 1590 nm ($\varepsilon = 35$ M^{-1} cm^{-1}) and 1673 nm ($\varepsilon = 20$ M^{-1} cm^{-1}). Since there are no f–f-transitions expected in hexavalent uranium complexes, the origin of these bands is uncertain. It is assumed that these faint features origin from interactions of traces (3%) of paramagnetic hydroxido **7** with the oxido **8** in solution, since **7** is also present in the ^{1}H NMR spectrum of **8**. The spectrum of **9** in benzene looks like a typical uranium(IV) ion indicating a successful one-electron reduction of **6** with KC_8 (Fig. S46,† top). It is noteworthy, that measuring **9** in THF leads to a different absorption. Now the spectrum of **9** and **4** are superimposable suggesting the solvation of the potassium ion and similar molecular and electronic structures of **4** and **9** in THF solution. This observed structural similarity is also supported by magnetic measurements (Fig. 8, bottom). The strong temperature dependence and the low magnetic moment $\mu_{eff} = 0.70$ μ_B at 2 K rather fit to a uranium(IV) complex and is also comparable to that of **4** (0.77 μ_B). In contrast to that, complex **7** is clearly identified as a uranium(V) complex with μ_{eff} values ranging from 0.97 μ_B at 2 K to 2.02 μ_B at 300 K.

Conclusions

In summary, and motivated by our recently reported hydroxido and oxido uranium complexes as active catalysts for the production of H_2 from water, we report the synthesis and coordination chemistry of a newly developed, hepta-dentate, cyclen-based tris(aryloxide) ligand precursor, namely cyclen(Me)($^{t\text{-Bu},t\text{-Bu}}$ArOH)$_3$, and its coordination chemistry to uranium. The resulting precursor complex [U^{III}((OAr$^{t\text{-Bu},t\text{-Bu}}$)$_3$(Me)cyclen)] (**1**) is more reactive than its previously reported, eight-coordinate, tetrakis-aryloxide derivative [U((OAr$^{t\text{-Bu},t\text{-Bu}}$)$_4$cyclen)], which could only be obtained in its tetravalent form.[44] Since it was not possible to obtain suitable crystals of **1** for single-crystal X-ray diffraction analysis, trivalent **1** was oxidized to the corresponding uranium(IV) complexes [(cyclen(Me)($^{t\text{-Bu},t\text{-Bu}}$ArO)$_3$)U^{IV}(Cl)] (**2**) and [(cyclen(Me)($^{t\text{-Bu},t\text{-Bu}}$ArO)$_3$)U(F)] (**3**) to draw conclusions about the precursor's molecular structure.

As expected, trivalent **1** is capable of reductively activating small molecules, such as H_2O and N_2O, yielding the tetravalent [(cyclen(Me)($^{t\text{-Bu},t\text{-Bu}}$ArO)$_3$)U^{IV}(OH)] (**4**) and pentavalent [(cyclen(Me)($^{t\text{-Bu},t\text{-Bu}}$ArO)$_3$)U^{V}(O)] (**7**) complexes, respectively. The solid-state molecular structures of these mononuclear complexes feature an N_4O_3X coordination mode, where the additional ligands (X = F, Cl, OH, O) bind in the equatorial position. Oxidation of **3** and **4** with AgF or $AgSbF_6$ yields the corresponding uranium(V) complexes [(cyclen(Me)($^{t\text{-Bu},t\text{-Bu}}$ArO)$_3$)U^{V}(F)$_2$] (**5**) and [(cyclen(Me)($^{t\text{-Bu},t\text{-Bu}}$ArO)$_3$)U^{V}(OH)][SbF$_6$] (**7**). Oxidation and reduction of **6** was achieved by a reaction with $AgSbF_6$ or potassium graphite; thus, providing access to hexavalent [(cyclen(Me)($^{t\text{-Bu},t\text{-Bu}}$ArO)$_3$)U^{VI}(O)][SbF$_6$] (**8**) and a tetravalent species, identified as [K][(cyclen(Me)($^{t\text{-Bu},t\text{-Bu}}$ArO)$_3$)U(O)] (**9**), respectively. Thus, the present study provides controlled and reproducible access to the first U(IV/V) hydroxido (**4** and **7**) and U(IV/V/VI) oxido (**6**, **8** and **9**) complex pairs in a retained ligand environment. Regardless, these complexes could not be used for the electrocatalytic production of H_2 from water.

Data availability

ESI† with general considerations, synthetic and spectroscopic details, NMR spectroscopy, IR vibrational spectroscopy, UV/Vis/NIR electronic absorption spectroscopy, VT SQUID magnetization spectroscopy, cyclic voltammetry, and single crystal X-ray structure determinations (PDF).

Author contributions

J. H. synthesized the ligand, and J. H. and S. T. L. synthesized the complexes, collected most of the spectroscopic, magnetochemical and electrochemical data. A. S. collected and analyzed the VT-VF NMR spectroscopic data during the revision process. F. W. H. collected and analyzed the crystallographic data. K. M. supervised and directed the project, edited and revised the manuscript.

Conflicts of interest

There are no conflicts to declare.

Acknowledgements

This work was supported by funds of the Bundesministerium für Bildung und Forschung (*f*-Char, BMBF support code 02NUK059E). We also thank the Friedrich-Alexander-Universität Erlangen-Nürnberg (FAU) for generous financial support.

Notes and references

1 J. Selbin and J. D. Ortego, *Chem. Rev.*, 1969, **69**, 657–671.
2 G. Kniewald and M. Branica, *Mar. Chem.*, 1988, **24**, 1–12.
3 D. E. Morris, *Inorg. Chem.*, 2002, **41**, 3542–3547.
4 I. Korobkov and S. Gambarotta, in *Progress in Inorganic Chemistry*, ed. K. D. Karlin, John Wiley & Sons, Inc, Hoboken, NJ, USA, 2005, pp. 321–348.
5 R. G. Denning, *J. Phys. Chem. A*, 2007, **111**, 4125–4143.
6 C. R. Graves and J. L. Kiplinger, *Chem. Commun.*, 2009, 3831–3853.

Open Access Article. Published on 12 August 2022. Downloaded on 1/22/2026 11:04:29 AM.
This article is licensed under a Creative Commons Attribution-NonCommercial 3.0 Unported Licence.

7 G. Wang, W. Um, Z. Wang, E. Reinoso-Maset, N. M. Washton, K. T. Mueller, N. Perdrial, P. A. O'Day and J. Chorover, *Environ. Sci. Technol.*, 2017, **51**, 11011–11019.
8 J. Berthet, M. Ephritikhine, M. Lance, M. Nierlich and J. Vigner, *J. Organomet. Chem.*, 1993, **460**, 47–53.
9 W. W. Lukens, S. M. Beshouri, L. L. Blosch and R. A. Andersen, *J. Am. Chem. Soc.*, 1996, **118**, 901–902.
10 P. Roussel, R. Boaretto, A. J. Kingsley, N. W. Alcock and P. Scott, *J. Chem. Soc., Dalton Trans.*, 2002, 1423–1428.
11 L. Karmazin, M. Mazzanti and J. Pécaut, *Inorg. Chem.*, 2003, **42**, 5900–5908.
12 K. A. N. S. Ariyaratne, R. E. Cramer, G. B. Jameson and J. W. Gilje, *J. Organomet. Chem.*, 2004, **689**, 2029–2032.
13 G. H. John, I. May, C. A. Sharrad, A. D. Sutton, D. Collison, M. Helliwell and M. J. Sarsfield, *Inorg. Chem.*, 2005, **44**, 7606–7615.
14 L. Natrajan, M. Mazzanti, J.-P. Bezombes and J. Pécaut, *Inorg. Chem.*, 2005, **44**, 6115–6121.
15 P. L. Arnold, C. J. Stevens, J. H. Farnaby, M. G. Gardiner, G. S. Nichol and J. B. Love, *J. Am. Chem. Soc.*, 2014, **136**, 10218–10221.
16 D. P. Halter, F. W. Heinemann, J. Bachmann and K. Meyer, *Nature*, 2016, **530**, 317–321.
17 M. W. Rosenzweig, A. Scheurer, C. A. Lamsfus, F. W. Heinemann, L. Maron, J. Andrez, M. Mazzanti and K. Meyer, *Chem. Sci.*, 2016, **7**, 5857–5866.
18 M. W. Rosenzweig, J. Hümmer, A. Scheurer, C. A. Lamsfus, F. W. Heinemann, L. Maron, M. Mazzanti and K. Meyer, *Dalton Trans.*, 2019, **48**, 10853–10864.
19 S. T. Löffler and K. Meyer, in *Comprehensive Coordination Chemistry III*, Elsevier, 2021, pp. 471–521.
20 D. P. Halter, F. W. Heinemann, L. Maron and K. Meyer, *Nat. Chem.*, 2018, **10**, 259–267.
21 Z. Zhang and R. M. Pitzer, *J. Phys. Chem. A*, 1999, **103**, 6880–6886.
22 G. Schreckenbach, P. J. Hay and R. L. Martin, *J. Comput. Chem.*, 1999, **20**, 70–90.
23 J. K. Gibson, R. G. Haire, M. Santos, J. Marçalo and A. Pires de Matos, *J. Phys. Chem. A*, 2005, **109**, 2768–2781.
24 M. L. Neidig, D. L. Clark and R. L. Martin, *Coord. Chem. Rev.*, 2013, **257**, 394–406.
25 N. Kaltsoyannis, *Inorg. Chem.*, 2000, **39**, 6009–6017.
26 N. Kaltsoyannis, *Chem. Soc. Rev.*, 2003, **32**, 9–16.
27 M. Pepper and B. E. Bursten, *Chem. Rev.*, 1991, **91**, 719–741.
28 T. W. Hayton, *Dalton Trans.*, 2018, **47**, 1003–1009.
29 S. C. Bart, C. Anthon, F. W. Heinemann, E. Bill, N. M. Edelstein and K. Meyer, *J. Am. Chem. Soc.*, 2008, **130**, 12536–12546.
30 B. Kosog, H. S. La Pierre, F. W. Heinemann, S. T. Liddle and K. Meyer, *J. Am. Chem. Soc.*, 2012, **134**, 5284–5289.
31 S. J. Kraft, J. Walensky, P. E. Fanwick, M. B. Hall and S. C. Bart, *Inorg. Chem.*, 2010, **49**, 7620–7622.
32 S. Fortier, J. L. Brown, N. Kaltsoyannis, G. Wu and T. W. Hayton, *Inorg. Chem.*, 2012, **51**, 1625–1633.
33 C. J. Hoerger, H. S. La Pierre, L. Maron, A. Scheurer, F. W. Heinemann and K. Meyer, *Chem. Commun.*, 2016, **52**, 10854–10857.
34 S. M. Franke, B. L. Tran, F. W. Heinemann, W. Hieringer, D. J. Mindiola and K. Meyer, *Inorg. Chem.*, 2013, **52**, 10552–10558.
35 D. S. J. Arney and C. J. Burns, *J. Am. Chem. Soc.*, 1993, **115**, 9840–9841.
36 D. M. King, F. Tuna, J. McMaster, W. Lewis, A. J. Blake, E. J. L. McInnes and S. T. Liddle, *Angew. Chem, Int. Ed*, 2013, **52**, 4921–4924.
37 N. Tsoureas, A. F. R. Kilpatrick, C. J. Inman and F. G. N. Cloke, *Chem. Sci.*, 2016, **7**, 4624–4632.
38 G. Zi, L. Jia, E. L. Werkema, M. D. Walter, J. P. Gottfriedsen and R. A. Andersen, *Organometallics*, 2005, **24**, 4251–4264.
39 W. J. Evans, S. A. Kozimor and J. W. Ziller, *Polyhedron*, 2004, **23**, 2689–2694.
40 J. L. Brown, S. Fortier, R. A. Lewis, G. Wu and T. W. Hayton, *J. Am. Chem. Soc.*, 2012, **134**, 15468–15475.
41 T. W. Hayton, *Chem. Commun.*, 2013, **49**, 2956–2973.
42 O. Cooper, C. Camp, J. Pécaut, C. E. Kefalidis, L. Maron, S. Gambarelli and M. Mazzanti, *J. Am. Chem. Soc.*, 2014, **136**, 6716–6723.
43 P. Waldschmidt, C. J. Hoerger, J. Riedhammer, F. W. Heinemann, C. T. Hauser and K. Meyer, *Organometallics*, 2020, **39**, 1602–1611.
44 J. Hümmer, F. W. Heinemann and K. Meyer, *Inorg. Chem.*, 2017, **56**, 3201–3206.
45 H. Nakai, K. Nonaka, T. Goto, J. Seo, T. Matsumoto and S. Ogo, *Dalton Trans.*, 2015, **44**, 10923–10927.
46 H. Nakai, J. Seo, K. Kitagawa, T. Goto, K. Nonaka, T. Matsumoto and S. Ogo, *Inorg. Chem.*, 2016, **55**, 6609–6615.
47 A. Rodríguez-Rodríguez, M. Regueiro-Figueroa, D. Esteban-Gómez, T. Rodríguez-Blas, V. Patinec, R. Tripier, G. Tircsó, F. Carniato, M. Botta and C. Platas-Iglesias, *Chem.– Eur. J.*, 2017, **23**, 1110–1117.
48 M. J. Monreal, R. K. Thomson, T. Cantat, N. E. Travia, B. L. Scott and J. L. Kiplinger, *Organometallics*, 2011, **30**, 2031–2038.
49 A.-C. Schmidt, F. W. Heinemann, C. E. Kefalidis, L. Maron, P. W. Roesky and K. Meyer, *Chem.– Eur. J.*, 2014, **20**, 13501–13506.
50 I. Castro-Rodríguez, H. Nakai and K. Meyer, *Angew. Chem., Int. Ed.*, 2006, **45**, 2389–2392.
51 O. P. Lam, F. W. Heinemann and K. Meyer, *C. R. Chim.*, 2010, **13**, 803–811.
52 A. V. Nizovtsev, A. Scheurer, B. Kosog, F. W. Heinemann and K. Meyer, *Eur. J. Inorg. Chem.*, 2013, **2013**, 2538–2548.
53 O. P. Lam, S. M. Franke, H. Nakai, F. W. Heinemann, W. Hieringer and K. Meyer, *Inorg. Chem.*, 2012, **51**, 6190–6199.
54 H. S. La Pierre, M. Rosenzweig, B. Kosog, C. Hauser, F. W. Heinemann, S. T. Liddle and K. Meyer, *Chem. Commun.*, 2015, **51**, 16671–16674.
55 M. Gregson, E. Lu, D. P. Mills, F. Tuna, E. J. L. McInnes, C. Hennig, A. C. Scheinost, J. McMaster, W. Lewis, A. J. Blake, A. Kerridge and S. T. Liddle, *Nat. Commun.*, 2017, **8**, 14137.
56 H. S. La Pierre and K. Meyer, *Inorg. Chem.*, 2013, **52**, 529–539.
57 S. T. Liddle, *Angew. Chem., Int. Ed.*, 2015, **54**, 8604–8641.

 © 2022 The Author(s). Published by the Royal Society of Chemistry

Open Access Article. Published on 12 August 2022. Downloaded on 1/22/2026 11:04:29 AM.
This article is licensed under a Creative Commons Attribution-NonCommercial 3.0 Unported Licence.

58 E. Hashem, A. N. Swinburne, C. Schulzke, R. C. Evans, J. A. Platts, A. Kerridge, L. S. Natrajan and R. J. Baker, *RSC Adv.*, 2013, **3**, 4350–4361.
59 D. R. Kindra and W. J. Evans, *Chem. Rev.*, 2014, **114**, 8865–8882.
60 J. A. Seed, L. Birnoschi, E. Lu, F. Tuna, A. J. Wooles, N. F. Chilton and S. T. Liddle, *Chem*, 2021, **7**, 1666–1680.
61 F. Delano and S. Demir, *Chem*, 2021, **7**, 1686–1688.
62 Z. Gajek, J. Mulak and J. C. Krupa, *J. Solid State Chem.*, 1993, **107**, 413–427.
63 R. D. Fischer, R. V. Ammon and B. Kanellakopulos, *J. Organomet. Chem.*, 1970, **25**, 123–137.
64 A.-C. Schmidt, F. W. Heinemann, W. W. Lukens and K. Meyer, *J. Am. Chem. Soc.*, 2014, **136**, 11980–11993.
65 A. J. Lewis, P. J. Carroll and E. J. Schelter, *J. Am. Chem. Soc.*, 2013, **135**, 511–518.
66 N. T. Rice, K. McCabe, J. Bacsa, L. Maron and H. S. La Pierre, *J. Am. Chem. Soc.*, 2020, **142**, 7368–7373.
67 T. W. Hayton, J. M. Boncella, B. L. Scott and E. R. Batista, *J. Am. Chem. Soc.*, 2006, **128**, 12622–12623.
68 E. Lu, O. J. Cooper, J. McMaster, F. Tuna, E. J. L. McInnes, W. Lewis, A. J. Blake and S. T. Liddle, *Angew. Chem., Int. Ed.*, 2014, **53**, 6696–6700.